Remote sources of water vapor forming precipitation on the Norwegian west coast at 60°N–a tale of hurricanes and an atmospheric river

A. Stohl,[1] C. Forster,[2] and H. Sodemann[1]

Received 25 May 2007; revised 10 August 2007; accepted 4 December 2007; published 11 March 2008.

[1] In September 2005, an extreme precipitation event occurred on the Norwegian southwest coast, which produced flooding and landslides and caused considerable infrastructure damage and loss of human life. We found that this event was triggered by the transport of tropical and subtropical moisture associated with two former hurricanes, Maria and Nate, which both underwent transition into extratropical cyclones. The two former hurricanes generated a large stream of (sub)tropical air which extended over more than 40° of latitude and across the North Atlantic Ocean and carried a large amount of moisture originally associated with hurricane Nate; a so-called atmospheric river or moisture conveyor belt. The mountains along the Norwegian coast caused a strong orographic enhancement of the precipitation associated with the moist air. A Lagrangian moisture tracking algorithm was employed to show that the evaporative source of the precipitation falling over Norway was distributed over large parts of the North Atlantic Ocean, and indeed included large contribution from the subtropics and smaller ones from the tropics. The moisture tracking algorithm was also applied over a 5-year period. It was found that (sub)tropical sources can contribute substantially to the precipitation falling in southwestern Norway throughout the year. Thus other transport mechanisms than hurricanes are important, too, for moving (sub)tropical moisture so far north. The (sub)tropical moisture source is relatively more important during the positive phase of the North Atlantic Oscillation, as well as for stronger precipitation events.

Citation: Stohl, A., C. Forster, and H. Sodemann (2008), Remote sources of water vapor forming precipitation on the Norwegian west coast at 60°N–a tale of hurricanes and an atmospheric river, *J. Geophys. Res.*, *113*, D05102, doi:10.1029/2007JD009006.

1. Introduction

[2] Precipitation amounts have increased in most areas of Norway during the period 1895–2004 [*Hanssen-Bauer*, 2005], consistent with an expected spin-up of the water cycle in a warming climate–temperatures in Norway have been increasing, too. There is a strong relationship between the North Atlantic Oscillation (NAO) [*Hurrell*, 1995] and precipitation in western Norway [*Uvo*, 2003]. Thus positive precipitation trends can be explained partly with a corresponding positive trend in the NAO. However, in southwestern Norway the precipitation trends are strongest in fall, whereas the NAO is most strongly correlated with precipitation in winter [*Hanssen-Bauer*, 2005]. Along with the monthly mean precipitation, heavy precipitation events have also become more frequent [*Groisman et al.*, 1999; *Alfnes and Førland*, 2006]. Downscaling of climate model predictions suggests that during the next few decades precipitation in Norway will increase further [*Benestad*, 2005], particularly in the western parts of the country [*Hanssen-Bauer et al.*, 2003]. Similar to the already observed changes, the predicted increase in precipitation along the Norwegian west coast is expected to be largest in fall, for which 2030–2049 precipitation amounts are forecasted to be about 15–25% greater than those in 1980–1999 [*Hanssen-Bauer et al.*, 2003]. Given these observed and predicted trends, it is important to understand the relevant precipitation processes, including where the water vapor forming the precipitation evaporates.

[3] We study precipitation in the southwestern part of Norway, around the city of Bergen, which receives the largest annual precipitation sums of the entire country, in excess of 3000 mm/a for the period 1961–1990. This remarkably large amount for such a high latitude region (Bergen is located at 60.5°N) is due to its coastal location at the end of the North Atlantic stormtrack and a strong orographic precipitation enhancement. Evaporation rates in the northeastern North Atlantic are moderate and we, thus, expect that much of the water falling as precipitation in southwestern Norway might have traveled over relatively long distances from the southwestern North Atlantic where evaporation rates are higher. However, to our knowledge this has never been investigated before. *Newell et al.* [1992] coined the term "tropospheric rivers" for bands of espe-

[1]Norwegian Institute for Air Research (NILU), Kjeller, Norway.
[2]Institute for Atmospheric Physics, German Aerospace Center, Oberpfaffenhofen, Germany.

0148-0227/08/2007JD009006$09.00

cially large vertically integrated water vapor (VIWV) fluxes (An alternative term used for the same [*Bao et al.*, 2006] or similar [*Knippertz and Martin*, 2007] features is "moisture conveyor belts".), which are of a similar magnitude as the water mass flux of the Amazon river and also have a similar length scale. *Zhu and Newell* [1998] showed that more than 90% of the total meridional water vapor transport in the midlatitudes occurs in these atmospheric rivers, although they cover less than 10% of the total area of the globe. Atmospheric rivers are normally connected to midlatitude cyclones [*Bao et al.*, 2006]. The water vapor originates in the warm sector south of the cyclone center [*Bao et al.*, 2006], converges along the trailing cold front [*Ralph et al.*, 2005], and finally feeds the so-called warm conveyor belt (WCB), which produces precipitation and, thereby, terminates the atmospheric river flow [*Eckhardt et al.*, 2004]. Not all bands of large VIWV flux are associated to midlatitude cyclones, though; some can also be associated with cut-off lows in the subtropics [*Knippertz and Martin*, 2007], and in this paper we will study a case associated with two hurricanes undergoing extratropical transition.

[4] Most of the water vapor in atmospheric rivers is contained in the lower troposphere. When such a river flows toward a mountain range, precipitation rates can be extreme, as has been shown for California [*Ralph et al.*, 2004, 2005]. *Ralph et al.* [2006] have shown that all flood events of the Californian "Russian River" during an eight year time period were associated with atmospheric rivers impinging on the coastal mountains.

[5] Except for a more than 20° difference in latitude, the situations in California and in western Norway are very similar. Both regions are located on the western continental margins; both coastlines are facing toward the west-southwest and, thus, are perpendicular to the most frequent flow direction of atmospheric rivers [*Ralph et al.*, 2004]; and both have a high coastal mountain range, leading to strong orographic precipitation enhancement. *Bao et al.* [2006] have suggested that atmospheric rivers over the Californian west coast tap into the tropical moisture reservoir. Here we demonstrate that transport of tropical or at least subtropical moisture was a critical factor for an extreme precipitation event in Norway, located more than 20° further north. By analyzing also data from a 5-year period, we then show that evaporation in the subtropics contributes substantially to the precipitation falling in southern Norway also in the "climatological" average.

2. Methods

[6] To determine where the water falling as precipitation over Norway originates from, we applied a Lagrangian method developed and validated by *Stohl and James* [2004, 2005] and used recently also by *Nieto et al.* [2006, 2007]. A similar method was developed recently by *Sodemann et al.* [2008] and both methods were inspired by the case study of *Wernli* [1997]. Our method is based on the calculation of a large number of trajectories with the Lagrangian particle dispersion model FLEXPART [*Stohl et al.*, 1998; *Stohl et al.*, 2005]. FLEXPART uses data from the European Centre for Medium-Range Weather Forecasts [*ECMWF*, 2002] to calculate both the grid-scale advection as well as the turbulent and convective transport of so-called particles. At the model start, the particles are distributed homogeneously in the atmosphere according to the distribution of atmospheric mass. Then, they are allowed to move with the mass-consistent winds and based on mass-consistent turbulence and convection parameterizations. As they move, the particles' mass remains constant (and, thus, also total atmospheric mass, which is an approximation). Values of the specific humidity q are interpolated to the particle positions from the ECMWF analysis grid, and the particle positions and q values are written to output files at a regular interval.

[7] Changes of q with time t can be used to diagnose the moisture budget of a particle along its trajectory,

$$e - p = m\frac{dq}{dt}, \tag{1}$$

where m is the particle's mass and e and p are the rates of moisture increases (evaporation) and decreases (precipitation) along the trajectory, respectively. By solving equation (1) for all particles and amassing $e - p$ over all K particles residing in the atmospheric column over an area A, the surface net freshwater flux

$$E - P \approx \frac{\sum_{k=1}^{K}(e-p)}{A} \tag{2}$$

is obtained.

[8] The equation (2) is an analogon to the Eulerian budget equation

$$E - P = \frac{\partial w}{\partial t} + \nabla \cdot \frac{1}{g}\int_0^{p_s} q\,\mathbf{v}\,dp, \tag{3}$$

where $w = \frac{1}{g}\int_0^{p_s} q\,dp$ is the precipitable water, g is the gravitational acceleration, p_s is the surface pressure, $\mathbf{v}$ is the wind, and E and P are the evaporation and precipitation rates per unit area, respectively [*Trenberth and Guillemot*, 1998]. *Stohl and James* [2004] have shown that when using a large enough number of particles, our Lagrangian method (equations (1) and (2)) gives results that are practically identical to the more widely used Eulerian method (equation (3)). Both methods have the disadvantage that they cannot disentangle E and P but the advantage that they are based only on observed quantities analyzed by the ECMWF on a grid.

[9] The advantage of the Lagrangian over the Eulerian method is that it can be used for tracking the $E - P$ budget also for selected particles only. For instance, using appropriate criteria, we can identify the particles contributing to a precipitation event, and track them backward in time, to identify where and when these so-called target particles have received moisture input prior to the event. Applying equation (2) along the trajectories of the target particles yields an $E - P$ distribution under the condition that the particles fulfill the target criteria, subsequently referred to as $(E - P)_c$. Because the target particles do not "fill" the entire atmospheric column, $(E - P)_c$ values do not represent the

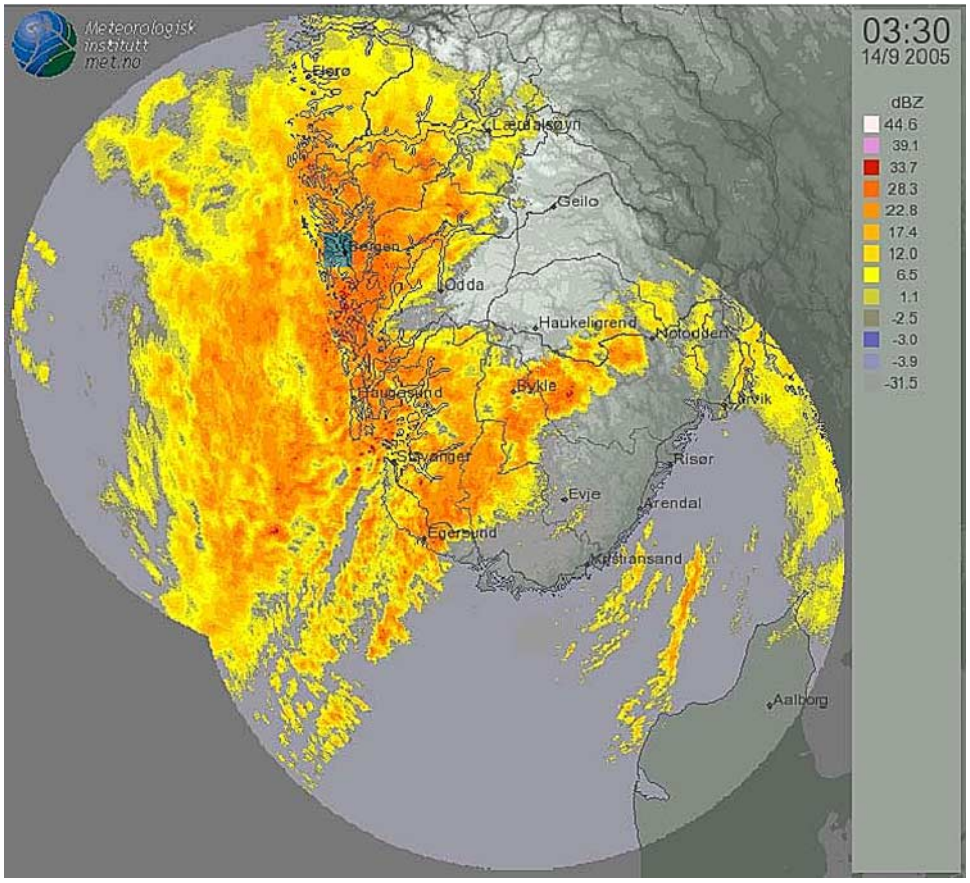

Figure 1. Radar reflectivities (dBZ) from the Norwegian precipitation radar network showing the distribution of rain over southwestern Norway on 14 September at 1:30 UTC. The location of Bergen is marked with a grey square.

surface net freshwater flux, but only the net freshwater flux into the air mass traveling to the target. $(E - P)_c$ values can be calculated for a certain point back in time, or can be integrated over a certain period backward from when the target criteria were fulfilled. To distinguish these two forms, we use the nomenclature $(E - P)_c^t$ to show $(E - P)_c$ at time t (given in days), and $(E - P)_c^{t,i}$ to show $(E - P)_c$ integrated from time t (where t is negative for the backward tracking) to time 0. In deviation from *Stohl and James* [2005], we include the first time step of the tracking, i.e., the time step when the target criteria were fulfilled.

[10] Given a sufficiently large area of an atmospheric column, the effects of turbulence and convection on column-integrated properties can be neglected instantaneously. This is particularly the case since lateral mixing is less strong than vertical mixing which does not affect the column-integrated properties. Indeed, effects of turbulence are ignored with the Eulerian method (equation (3)). However, when particles are tracked over a longer time, turbulence and convection significantly alter their trajectories, especially in the boundary layer and in convectively active regions. Initially, changes in a trajectory come about mostly through vertical displacements of a particle by active turbulence or convection, which subsequently also changes its horizontal position because horizontal winds vary with altitude. The time series of interpolated q values along a trajectory are changed implicitly, too by the displacements, and so is the term $\frac{dq}{dt}$ in equation (1). Since FLEXPART uses appropriate parameterizations, our method fully incorporates the effects of parameterized turbulence and convection.

[11] Two simulations were made: In the first simulation of the case-study period, particles were initialized in a relatively small target volume in southwestern Norway, which through appropriate generation of particles at the boundaries was kept full with particles over the 1.5 day duration of the precipitation event. In total, 0.9 million particles were initialized in the target volume and tracked for 15 days, with hourly particle position output. The second simulation was made for the period December 1999 until March 2005 and used a global set-up identical to that described by *Stohl and James* [2005], except that more particles (1.9 million) were used but only 6-hourly model output was produced. This data set was available from a previous study on transport into the Arctic [*Stohl*, 2006] and it was used for putting the moisture sources found for the case study into a ''climatological'' perspective.

[12] The number of particles used as well as the model output interval determine the spatiotemporal resolution that

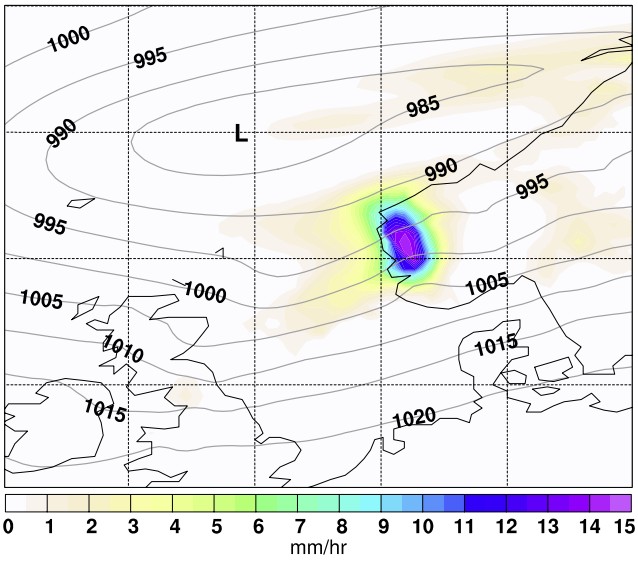

Figure 2. Precipitation rate (mm h^{-1}, color shading) on 14 September for 0–3 UTC from the ECMWF 0 UTC forecast, with superimposed 0 UTC sea level pressure analysis (hPa, isolines).

can be obtained with our method. 1.9 million globally distributed particles corresponds to about 30 particles in a 1° × 1° grid column. Ideally, the number of particles per grid column should be much larger than the number of vertical layers (60) in the ECMWF data, since the stochastic nature of the particle transport requires a large number of particles per ECMWF grid cell (say, 100) in order to preserve the full resolution of the input data. Therefore the climatological data set is unsuitable for case studies and at the full spatial resolution even monthly averages can still be noisy. We, therefore, present only seasonal averages over the 5-year period. For the case study simulation, only 0.9 million particles were used but they were released over an area of only 6° × 7°, yielding 360 particles per 1° × 1° grid column, which is suitable to preserve the full spatio-temporal resolution of the ECMWF data, even in the higher-resolution nest (see below).

[13] The ECMWF input data had 60 vertical levels and a resolution of 1° × 1°. For the case study, higher resolution data (0.36° × 0.36°) for the area (108°W–18°E, 18°N–72°N) was nested into the global data, taking advantage of the full resolution of the ECMWF model. In addition to the

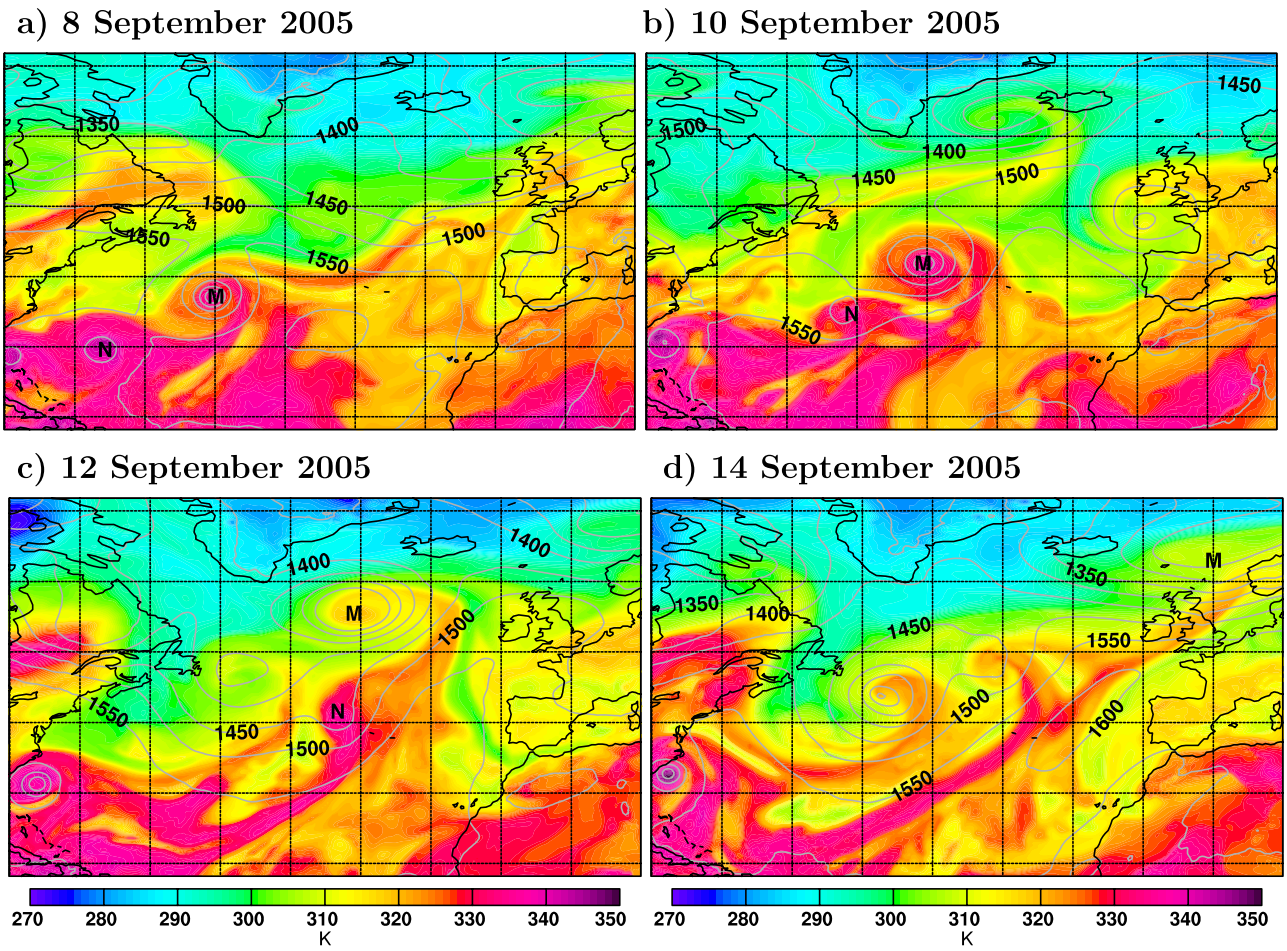

Figure 3. Equivalent potential temperature (in K, color shading) and geopotential height (in m, isolines) at 850 hPa on (a) 8, (b) 10, (c) 12, and (d) 14 September 2005, all at 0 UTC. The positions of (former) tropical cyclones Maria and Nate, taken from the reports of *Pasch and Blake* [2006] and *Stewart* [2005], are marked with the letters "M" and "N", respectively.

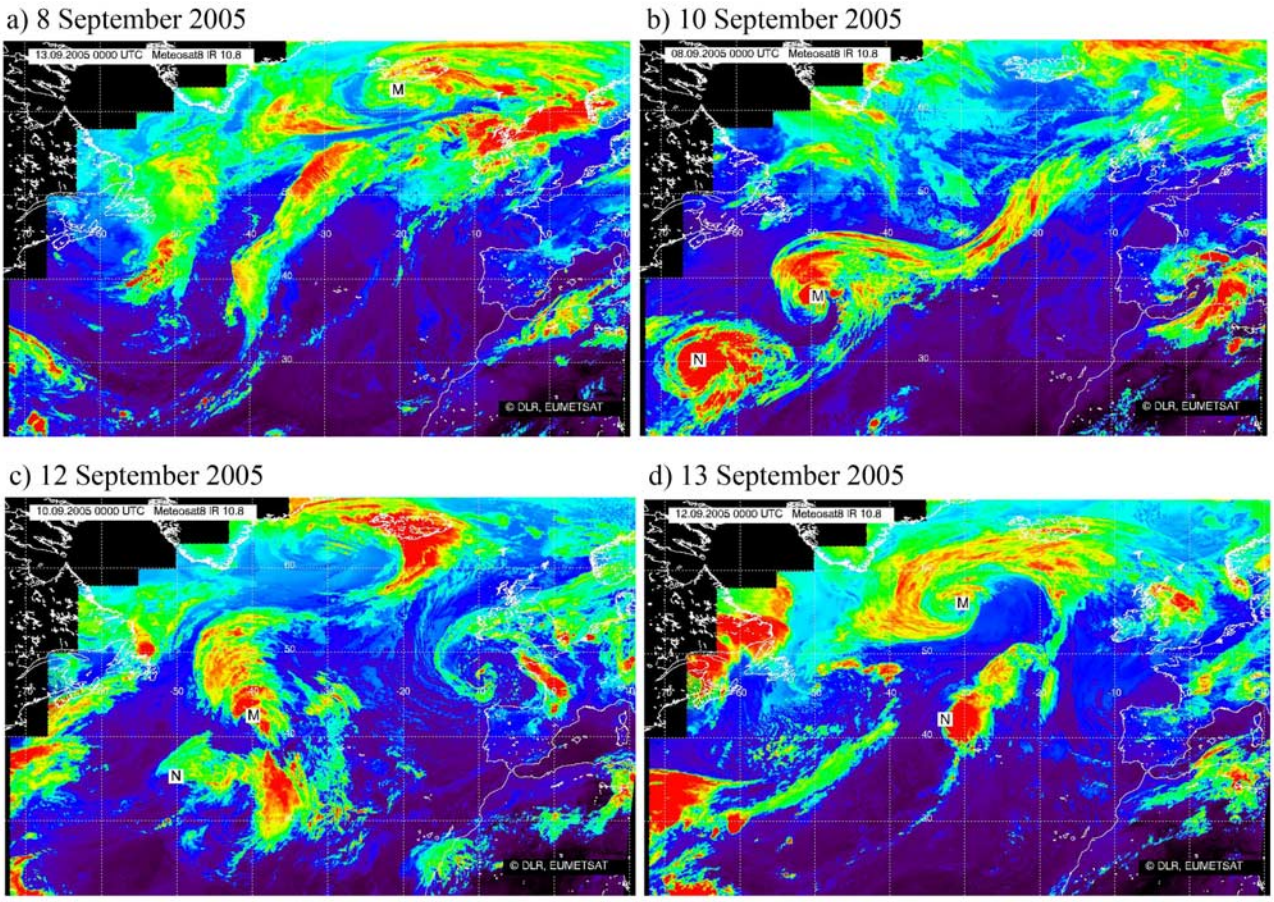

Figure 4. Meteosat-8 infrared brightness temperatures in the 10.8 μm channel on (a) 8, (b) 10, (c) 12, and (d) 13 September 2005, all at 0 UTC. Reddish colors indicate low cloud top temperatures (high cloud tops) with a minimum of 225 K, bluish colors indicate high cloud top temperatures with a maximum of 300 K. Black areas indicate missing data. The positions of (former) tropical cyclones Maria and Nate, taken from the reports of *Pasch and Blake* [2006] and *Stewart* [2005], are marked with the letters "M" and "N", respectively.

analyses at 0, 6, 12 and 18 UTC, 3-h forecasts at 3, 9, 15, and 21 UTC were used.

3. Case Study

3.1. Meteorological Overview

[14] During the night from 13 to 14 September 2005, the storm "Kristin" hit the Norwegian west coast and caused extreme precipitation, flooding and landslides. One person died and several persons were injured by a landslide that destroyed several houses in the city of Bergen. The flooding also caused considerable infrastructure damage. The weather station Bergen-Florida (5.3°E, 60.4°N) measured 156.5 mm precipitation within 24 h, 110.5 mm of which fell within 12 h. This was the largest daily precipitation amount measured since the station was established in the year 1875, and more than half the normal (1961–1990) monthly precipitation of 283 mm in September, the rainiest month of the year *Meteorological Institute* [2005]. Another station, Opstveit (6.0°E, 59.9°N), recorded a daily precipitation amount of 179.5 mm, the largest daily value ever measured in entire Norway in a September. A reflectivity map from the Norwegian precipitation radar network shows heavy rainfall along the Norwegian west coast on 14 September at 1:30 UTC (Figure 1). The precipitation was connected to a front approaching Norway rapidly from the west at 0 UTC and passing the Norwegian coast during the night. At 6 UTC, the rainfall was still strong but had already decreased considerably.

[15] The ECMWF sea level pressure analysis for 0 UTC (isolines in Figure 2) shows a low-pressure system located to the northwest of the area with heavy precipitation. The low-level onshore flow southeast of the cyclone center caused an extreme orographic precipitation enhancement over the western slope of the coastal mountain range. The 3-h forecast from 0 UTC shows that the ECMWF model captured the event very well, with almost 50 mm of 3-hourly accumulated precipitation over the mountains (color shading in Figure 2).

[16] The low pressure system developed out of hurricane "Maria" and an extratropical cyclone over the Norwegian Sea, as described by *Pasch and Blake* [2006]. Maria originated in the tropical Atlantic by the end of August 2005, traveled north-westward until 7 September and then north-

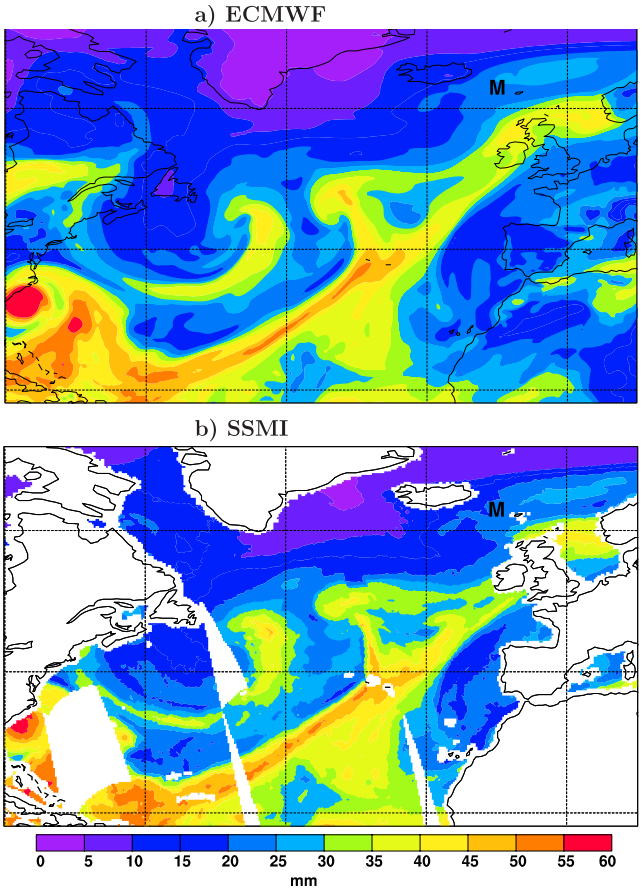

Figure 5. Maps of the vertically integrated water vapor from (a) the ECMWF analysis on 13 September 2005 at 18 UTC and (b) the SSM/I measurements made during the afternoon overpasses on 13 September 2005. SSM/I retrievals are made only over the oceans.

eastward. On 8 September, Maria was characterized by a deep geopotential height minimum (Figure 3a) but the cloud bands associated with it were not well organized anymore (Figure 4a). By 10 September, Maria had been transformed into an extratropical cyclone (Figure 3b) with a poorly defined frontal cloud system (Figure 4b). In response to strong baroclinic forcing, however, the storm re-intensified and again acquired hurricane-force winds on 11 September. At that time, the cloud structures were again almost hurricane-like. Winds began weakening on 12 September as the system grew in size (Figures 3c and 4c) and when Maria passed near Iceland on 13 September (Figure 4d). Finally, as the system approached Norway on 14 September (Figure 3d), it merged with a trough over the Norwegian Sea, grew further in size and caused the flooding as the storm called Kristin.

[17] Maria's core was warm and moist and, thus, featured a maximum of the equivalent potential temperature Θ_e in the lower troposphere (Figure 3). However, on 12 September (Figure 3c) the Θ_e maximum was not particularly strong anymore, and it decreased further on the following day. More importantly, though, warm and moist air was also located first to the southwest (Figures 3a–3b) and then to the south (Figures 3c–3d) of Maria. It was associated with another hurricane, "Nate", described by *Stewart* [2005], that developed shortly after Maria (Figure 3). On 8 September, hurricane Nate had well-defined cloud bands (Figure 4a). However, after undergoing extratropical transition, Nate never appeared as a strong minimum in the geopotential height (Figures 3b–3c). The clouds associated with Nate were deep but did not extend over a large area (Figures 4b–4c). Note that the clouds east of 40°W on 10 September (Figure 4b) and east of 25°W on 12 September (Figure 4c) were associated with Maria, not Nate. Because Nate's cloud system was small and rain formation was limited to a small area, the tropical character of the air associated with Nate was well preserved. The larger system Maria steered this warm and moist air rapidly to the northeast. One could also say that the tropical air that had been moved northward as part of Nate was handed over to Maria which transported it even further north. On 13 September, deep clouds started forming in the tropical air over the northern part of the British Isles and toward Norway as the warm moist air was incorporated into the frontal system of Kristin (Figure 4d), which was just developing out of Maria.

[18] On 14 September (Figure 3d), a long band of high Θ_e air stretched from the Caribbean all the way across the North Atlantic to the Norwegian west coast, spanning more than 40° of latitude. This band was characterized by high values of VIWV, reminiscent of an atmospheric river [*Newell et al.*, 1992]. Figure 5 shows excellent agreement between VIWV obtained from the ECMWF 13 September 18 UTC analysis (Figure 5a) and VIWV retrieved from the Special Sensor Microwave/Imager (SSM/I) using version 6 of the algorithm originally described by *Wentz and Spencer* [1998] from the 13 September afternoon overpasses (Figure 5b). Both data sets show distinctly elevated VIWV values west of the Norwegian coast that were connected to the Caribbean by the atmospheric river.

[19] Figure 6 shows maps of the horizontal VIWV flux. Strong circular fluxes (dark areas) are associated with the hurricanes Maria and Nate on 8 September (Figure 6a). On 10 September (Figure 6b), the two systems Maria and Nate were so close to each other that the water vapor fluxes on their southeastern sides merged (note, however, that the air masses associated with Maria and Nate can still be clearly separated). This resulted in a single circulation feature, which grew rapidly in size on 12 September (Figure 6c) and eventually formed the band of strong northeastward VIWV flux, the atmospheric river, covering almost the entire North Atlantic (Figure 6d). When the VIWV flux maximum reached the Norwegian coastline, the mountain range quickly extracted moisture from the already precipitating airstream, thus leading to the flooding.

[20] Figures 7a and 7c show vertical cross-sections along 20°W on 13 September at 0 UTC through the core of Maria/Kristin. A large potential vorticity (PV) tower *Wernli et al.* [2002] is apparent throughout the middle troposphere at about 62°N (red 2 pvu contour in Figure 7a) and a narrow tropopause fold is reaching down south of the PV tower. The PV tower appears to be sustained by intense diabatic heat release in the WCB, as indicated by the high-reaching liquid water and ice clouds (Figure 7a, blue contours) and the strong vertical upward motion to the north of the

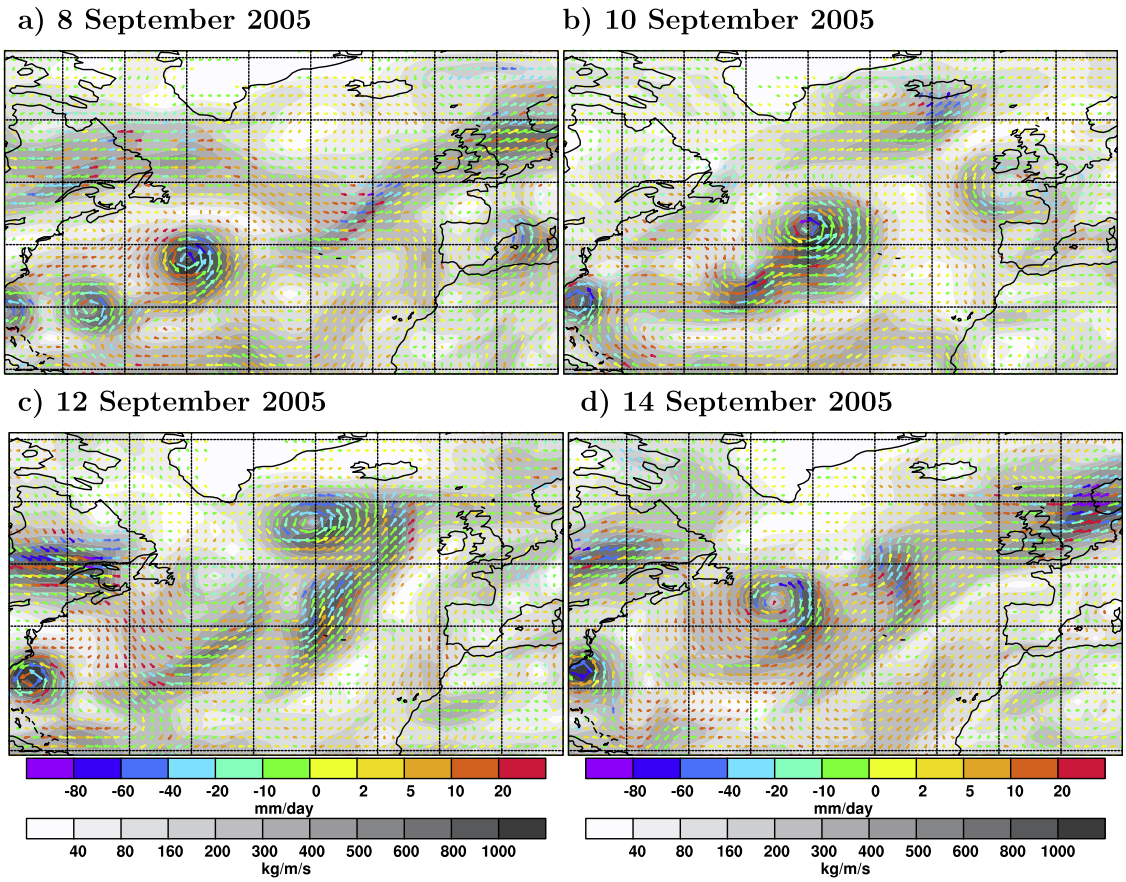

Figure 6. Maps for (a) 8, (b) 10, (c) 12, and (d) 14 September 2005, all at 0 UTC, of the vertically integrated horizontal flux of water vapor calculated from the ECMWF analyses. The grey shading gives the magnitude of the flux and the arrows indicate its direction, with the arrows' length also indicating the magnitude. Arrows are color coded according to the net surface freshwater flux $E - P$ diagnosed from the ECMWF analyses.

cyclone center (Figure 7c, yellow contours). South of the low-level horizontal water vapor flux maximum near 60°N at 150 m altitude (Figure 7c, white contours), which is part of Kristin, a second, stronger maximum of horizontal water vapor flux is apparent near 47°N at 600 m altitude. This is the somewhat elevated atmospheric river (or moisture conveyor belt) associated with Nate.

[21] One day later, on 14 September at 0 UTC, a vertical cross section along 5°E (approximately the longitude of Bergen) exhibits fragments of Kristin's decaying PV tower (Figure 7b). Signatures of extremely strong convection, i.e., strong upward motion up to the tropopause (Figure 7d) and high values of cloud liquid and ice water content (Figure 7b) can be found around 60°N and explain the strong precipitation rates. The water flux maximum near 57°N and at about 400 m altitude is just south of where the extreme convection occurred. Even stronger water fluxes (>0.4 kg m^{-2} s^{-1}) occurred further west at earlier times, before the water vapor maximum was eroded by the strong convection and the resulting precipitation. In Figure 7d, the moisture fluxes associated with Nate and Maria/Kristin are not as well separated from each other as on the previous day (Figure 7c). However, series of such sections show that the high moisture fluxes seen in Figure 7d south of about 62°N were all associated with the (sub)tropical moisture of Nate. The moisture associated with Maria/Kristin itself is found further north, from about 63°N to 70°N, with the flux minimum at 67°N occurring near Kristin's core. The two systems can be separated somewhat better in the relative humidity field, as well as in the cloud liquid and ice water content (Figure 7b), which all show two separate towers of convection. Thus we conclude from this analysis that the strongest precipitation was caused by the moisture associated with Nate. However, Maria/Kristin was also important as it channeled this moisture toward the Norwegian coast. It also contributed some precipitation north of Bergen.

3.2. Moisture Source Regions

[22] In the following, we use the method of *Stohl and James* [2004, 2005] to identify where the moisture that rained out over southwestern Norway, had evaporated. For this, we must first objectively identify "particles" contributing to the precipitation event. We considered the target region 2–8°E and 58–65°N for the time period 13 September 12 UTC to 14 September 15 UTC. Practically all of the precipitation fell in that area during this time period. We calculated hourly $E - P$ values on a $1° \times 1°$ grid in this target area and considered only particles in grid cells where and when $E - P < -2$ mm hr^{-1}. This excluded areas and times with light or no precipitation, which occurred especially in the

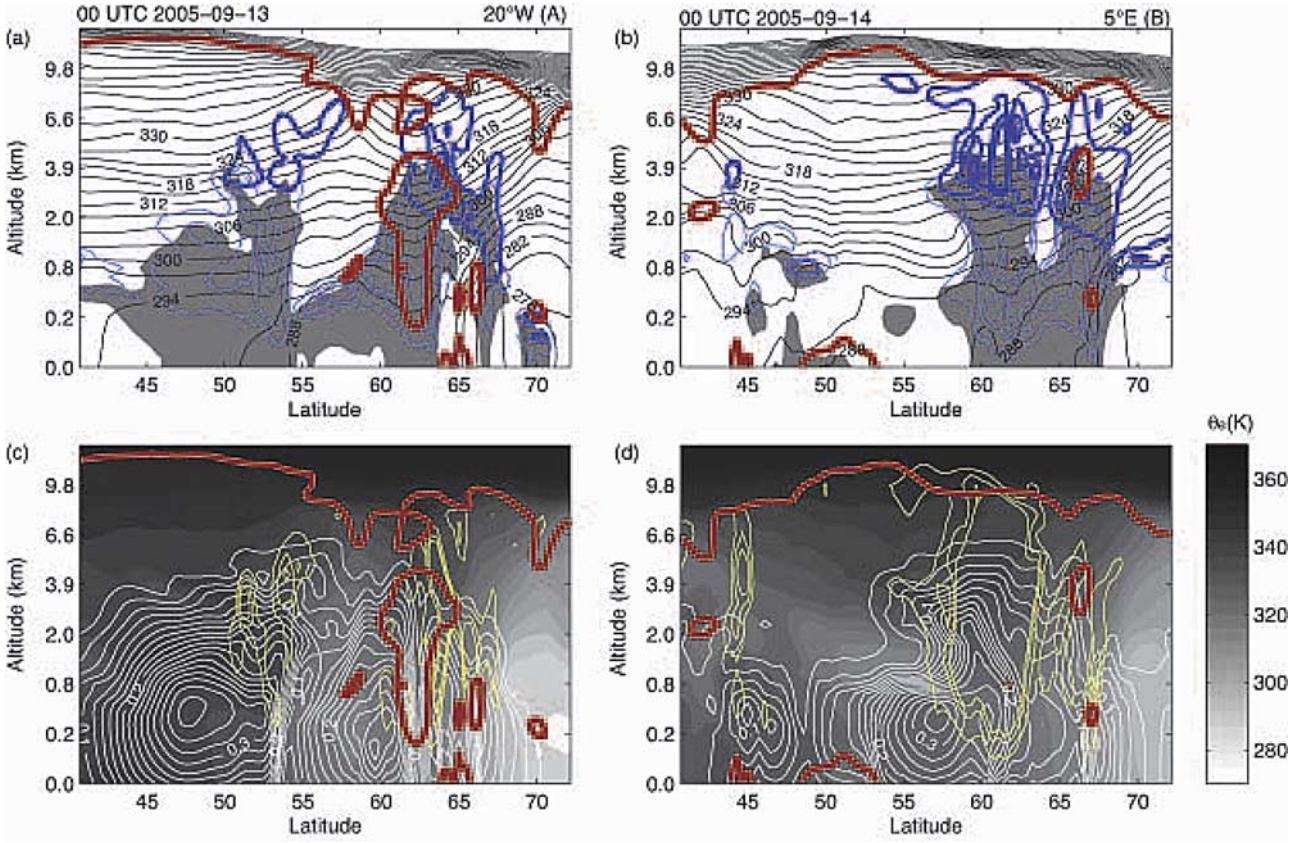

Figure 7. Vertical cross-sections showing the moisture flux configurations (a, c) along 20°W on 13 September 2005 at 0 UTC and (b, d) along 5°E on 14 September 2005 at 0 UTC. Top panels (a, b): Isentropes (black contours), relative humidity >90% (shaded), cloud water >0.01 g kg^{-1} (thin blue contours, contour interval 0.05 g kg^{-1}), cloud ice >0.01 g kg^{-1} (thick blue contours, contour interval 0.05 g kg^{-1}), potential vorticity = 2 pvu (red contour). Lower panels (c, d): equivalent-potential temperature Θ_e in K (shaded), horizontal moisture flux >0.02 kg m^{-2} s^{-1} (white contours, contour interval 0.02 kg m^{-2} s^{-1}), vertical velocity <−0.15 hPa s^{-1} (yellow contours, contour interval 0.15 hPa s^{-1}), potential vorticity = 2 pvu (red contour).

northernmost 2° of the target area as well as in large parts of the target area at the beginning and toward the end of the target period. Finally, particles with $\frac{dq}{dt} > 0$ g kg^{-1} hr^{-1} were removed, as they did not contribute to the precipitation. The remaining "target particles" (about 200,000) were tracked backward in time for 12 days.

[23] Figure 8 shows the trajectories of a small subset of the target particles, namely those with a particularly strong moisture decrease of $\frac{dq}{dt} < -3.5$ g kg^{-1} per 3 h between 0–6 UTC on 14 September. The precipitating air masses incorporated trajectories arriving from large parts of the North Atlantic Ocean. Midlatitude air was arriving in association with the trough with which Maria merged to form Kristin just before approaching Norway, and subtropical air was moving northeastward through the combined circulations of Nate and Maria. Both pathways were chiefly associated with moisture increases (net evaporation), except for their final section over the Northeastern Atlantic Ocean where strong moisture loss prevailed. Particularly strong moisture increases occurred over the subtropical North Atlantic where also the trajectory density was high.

[24] The trajectory plot, while informative, provides only qualitative information. Figure 9, therefore, shows maps of $(E-P)_c^{t,i}$ for all target particles, for four different times t of backward tracking. As expected, $(E-P)_c^{12,i}$ is strongly negative over southwestern Norway, with a minimum value of −120 mm. Given the relatively coarse 1° resolution of our analysis grid and considering that evaporation may have occurred, too, this is in reasonable agreement with the highest observed precipitation amounts of more than 150 mm. Considering the full 12 days of tracking (Figure 9d), a band of strongly negative $(E-P)_c^{12,i}$ values stretches back to about 30°W and 40°N and continues less clearly to 60°W and 30°N. Figure 9a shows that this band is largely due to precipitation occurring during the last 24 h before the air arrived in the target area, and a movie of 12-hourly $(E-P)_c^t$ maps (not shown) reveals very few negative $(E-P)_c^t$ values occurring earlier than 2 days before arrival. During the last two days, on the other hand, positive $(E-P)_c^t$ values were rare and only found immediately to the south of the precipitation band (Figures 9a–9b; see also Figure 6d). These positive $(E-P)_c^t$ values in the eastern North Atlantic Ocean and North Sea contributed only a minor fraction of the moisture falling as precipitation in the target area, estimated at about 10% for the area east of 10°W. Nevertheless, it is clear that through convergence the precipitating atmospheric river was fed with

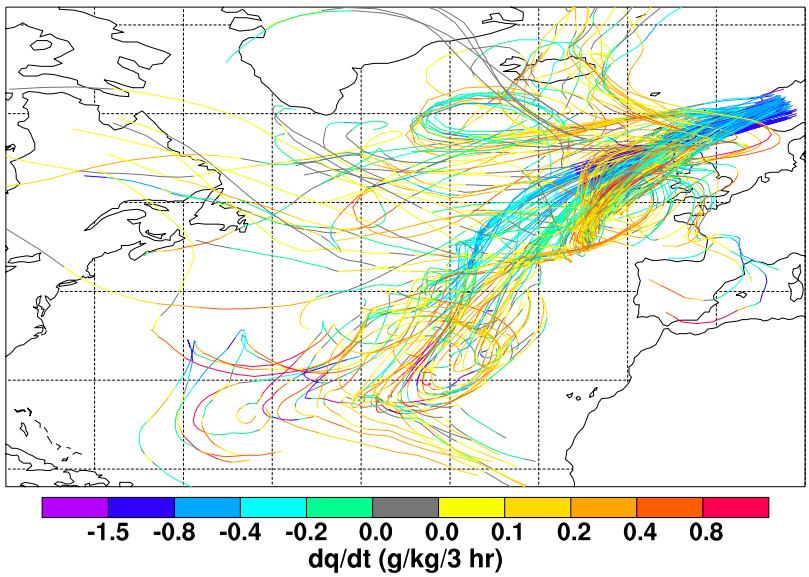

Figure 8. 12-day back trajectories of the particles arriving in grid cells with negative $E - P$ in the target region 2°E–8°E and 58°N–65°N between 0 and 6 UTC on 14 September 2005. Only the trajectories with a particularly strong moisture decrease of more than 3.5 g kg^{-1} over a 3-h period in the target region are shown. Trajectory segments are color coded according to the associated change of specific humidity.

moisture evaporated relatively close-by until it reached the Norwegian coastline. However, the dominant part of the moisture must have originated further away. Indeed, high $(E - P)_c^{12,i}$ values can be found over much of the western and central North Atlantic Ocean, both in the middle latitudes and in the subtropics (Figure 9d). Strongly positive $(E - P)_c^{12,i}$ values can be found at 20°N and even further south, indicating that some of the moisture was transported from the subtropics and even the tropics across more than 40° of latitude before precipitating out over southern Norway. Most of the moisture uptake was actually happening during the last 8 days (Figure 9c). Spatial $(E - P)_c^{t,i}$ patterns remain very similar when integrating over 12 days (Figure 9d), and even experiments with a 20-day tracking revealed no substantial differences, as so far back in time particles were dispersed over much of the Northern hemisphere, with no substantial moisture uptake occurring at any particular location.

[25] Figure 10 shows the change in the total mass of water vapor M_{WV} carried by all the target particles as a function of time before the target criteria were fulfilled. The mass change is displayed as the difference $\Delta M_{WV}(t) = M_{WV}(t) - M_{WV}(0)$, where $M_{WV}(t)$ is the total water vapor mass at some time t and $M_{WV}(0)$ is the total water vapor mass remaining after the target criteria were fulfilled. This quantity is obtained through spatial integration of $(E - P)_c^{t,i}$. Note that for the individual particles the target criteria were fulfilled at different times but time was counted from the time step when the target criteria were first met, resulting in a common time zero. When the target criteria were fulfilled for several subsequent time steps, this was accumulated at time zero. An increase of ΔM_{WV} (forward in time) indicates net evaporation (positive area-integrated $(E - P)_c^t$), whereas a decrease indicates net precipitation. ΔM_{WV} is increasing at an accelerating rate on days −12 to −4, remains constant on day −3, and drops rapidly on days −2 and −1. Almost half of the moisture decrease during the last two days occurred in the last 6 h, and 25% actually occurred when the target criteria were fulfilled.

[26] Figure 10 also shows the mass changes separately for six latitude bands in the Northern hemisphere. The moisture decrease during the last two days occurred mainly in the latitude bands 50–60°N and 60–70°N. Further back in time, there is little change in ΔM_{WV} in these latitude bands but a slow decrease is noticeable at 50–60°N. Latitude bands 30–40°N and 40–50°N show decreasing ΔM_{WV} on day −3, indicating the onset of precipitation, but increasing ΔM_{WV} and, thus, moisture uptake on earlier days. Strongly increasing ΔM_{WV} is also found in latitude band 20–30°N on days −12 to −4, and some increase (0.5 Gt in total) can even be seen at 10–20°N. This temporal evolution of ΔM_{WV} in the different latitude bands is consistent with the previously discussed strong evaporation in the (sub)tropics, transport of the moisture northward, onset of precipitation en route, which was fed additionally by convergence of moisture evaporated relatively close-by, and then the quick extraction of moisture by the topographically enhanced ascent during the last few hours.

4. "Climatological" Moisture Source Regions

[27] In order to put the severe precipitation event studied above into perspective, we used the 5-year data set. We tracked backward all particles with a moisture decrease in 1° × 1° grid cells of the target domain (the same domain as used above) with $E - P$ smaller than -3 mm per 6-h time step. This criterion is somewhat less strict than that used in the case study ($E - P < -2$ mm h^{-1}) because the 5-year model output was available only every six hours and also because otherwise very few precipitation events would have been identified. Figure 11 shows the climatological $(E - P)_c^{12,i}$ fields from the particle tracking. In the target domain, $(E - P)_c^{12,i}$ is the least negative in spring and the most

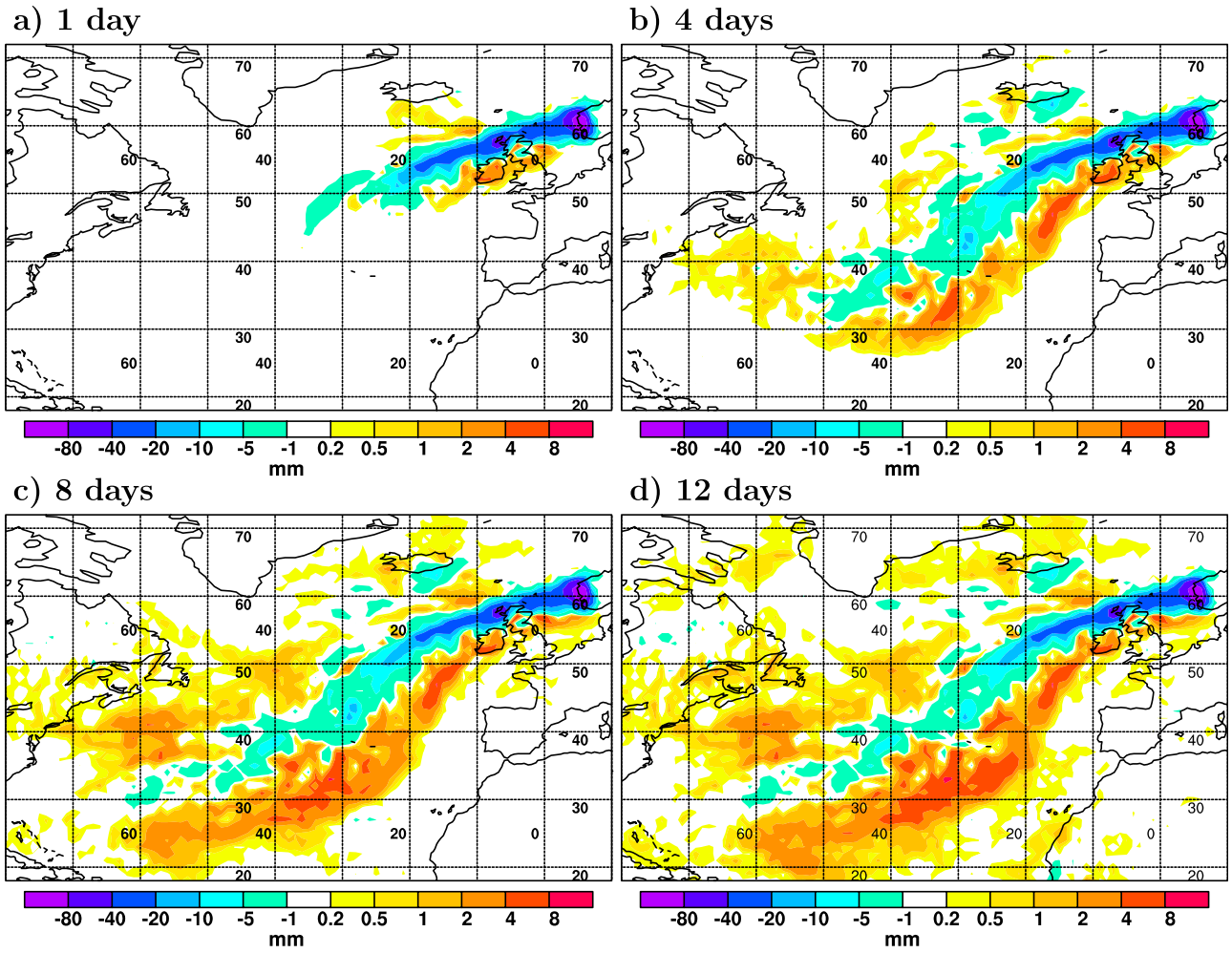

Figure 9. Values of $(E-P)_c^{1,i}$ (a), $(E-P)_c^{4,i}$ (b), $(E-P)_c^{8,i}$ (c) and $(E-P)_c^{12,i}$ (d), diagnosed from 12-day back trajectories of the target particles arriving in the region 2°E–8°E and 58°N–65°N between 6 UTC on 13 September and 15 UTC on 14 September 2005.

negative in fall, in agreement with the smallest and largest climatological precipitation amounts at the station Bergen-Florida during those seasons, respectively. Outside the target domain, $(E-P)_c^{12,i}$ values are generally positive, indicating net moisture uptake. An exception is the main "approach corridor", along which precipitation tends to occur already before the target particles reach the coastline. This is reminiscent of our case study.

[28] There is a marked difference in net moisture source regions between winter and summer (compare Figures 11a and 11c). In winter, positive $(E-P)_c^{12,i}$ values occur exclusively over the oceans, whereas in summer, $(E-P)_c^{12,i}$ values can be positive also above the continents. Especially the strongly positive $(E-P)_c^{12,i}$ values over Europe indicate that in summer, a significant fraction of the precipitation falling on Norway's southwest coast has a regional continental source. When considering Europe as a whole as a target area, this could be viewed as precipitation recycling [*Eltahir and Bras*, 1996] over the continent.

[29] It is remarkable that remote areas, such as the Gulf of Mexico, the start of the North Atlantic storm track off the eastern seaboard of North America, and the entire subtrop-

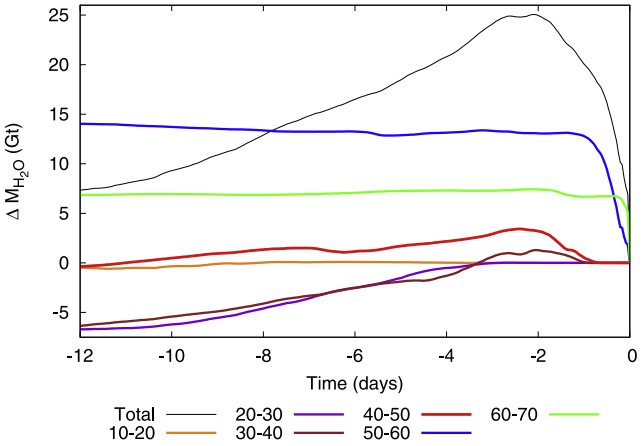

Figure 10. Change in the total mass of water vapor, ΔM_{WV}, carried by the target particles as a function of time backward from the time step when the target criteria were fulfilled. The total mass change is plotted as a black line. Mass changes contributed in six different latitude bands are shown separately by the colored lines.

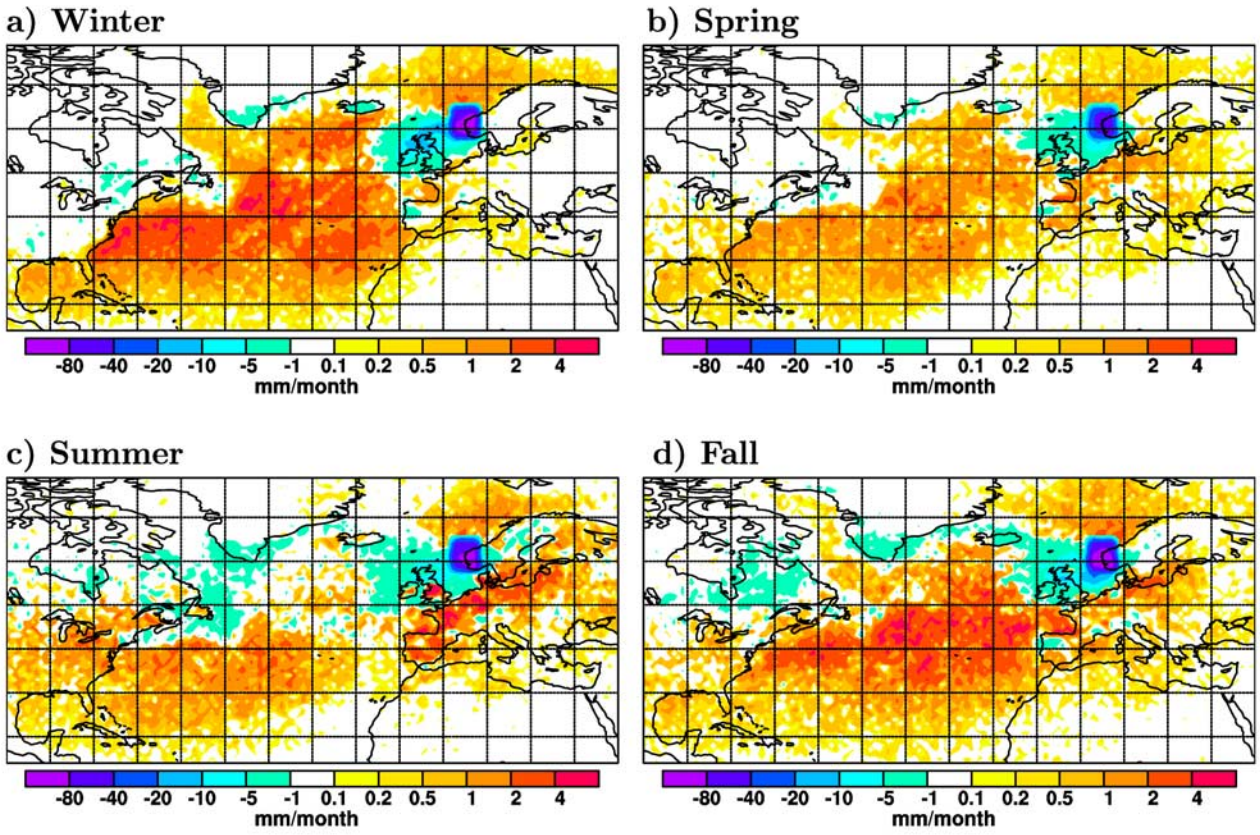

Figure 11. Values of $(E - P)_c^{12,i}$ from the 5-year particle tracking for (a) winter (December, January, February), (b) spring (March, April, May), (c) summer (June, July, August), and (d) fall (September, October, November).

ical North Atlantic, are substantial moisture source regions throughout the year. Also the Norwegian Sea is an important but much closer moisture source, due to cold and dry Arctic air masses being transported across the relatively warm ocean surface, en route to southwestern Norway. In summer, most of the moisture is contributed by ocean surfaces in the relatively narrow subtropical latitude band 20–40°N, whereas the midlatitudes are relatively less important. In winter, on the other hand, midlatitude source regions are almost as important as the subtropics. The tropical latitudes south of 20°N are a small net moisture source for southwestern Norway throughout the year. Though less important than the subtropics, the extremely long meridional transport from the tropics is remarkable. As the tropical source is also present in winter, hurricanes cannot be the only mechanism by which the tropical moisture is transported so far north. Atmospheric rivers associated with ''normal'' extratropical cyclones, similar to the cases studied for California [*Ralph et al.*, 2004, 2005; *Bao et al.*, 2006], are likely another important mechanism also for Norway.

[30] Our 5-year global data set is unsuitable for investigating extreme events because of a too low particle number density in the target region. However, we performed a sensitivity study by considering particles only when they lost more than 1 g kg^{-1} per 6-h time step in target grid cells with $E - P$ smaller than -6 mm per 6-h time step. Using these criteria, the relative evaporative contributions from the Norwegian Sea are reduced and those from the mid- and low-latitude North Atlantic are slightly increased over those obtained with the standard method. Thus it seems the low-latitude moisture sources are indeed more important for the stronger precipitation events; however, a regional simulation with higher particle density will be needed to confirm this.

[31] An interesting question is how the NAO influenced the moisture source regions. Unfortunately, the NAO was never in a strongly negative or positive state (see http://www.cgd.ucar.edu/cas/jhurrell/indices.html) during the 5 years covered by our data set. However, the winter (December until March) 2000 featured a moderately positive and the winter 2001 a moderately negative phase of the NAO. An analysis of the 4-month composites of these two winters shows that over the target region $E - P$ was more negative for the positive phase, in agreement with larger measured precipitation amounts. More importantly, $(E - P)_c^{12,i}$ values were much larger in the tropics and subtropics during the positive phase, indicating that low-latitude source regions are relatively more important during the positive NAO phase.

[32] Although not many studies on the moisture source regions of precipitation are available, two comparisons can be made. For precipitation over Iceland, *Nieto et al.* [2007] found remarkably similar source regions as we have identified, i.e., the southwestern North Atlantic south of about 45°N and, particularly, the Norwegian

Sea, which for Iceland seems to be even more important than for southwestern Norway. For winter precipitation over Greenland, *Sodemann et al.* [2008] found moisture sources to be located relatively close to the landmass of Greenland but, again, the Norwegian Sea as well as the northeastern North Atlantic were important source regions. *Sodemann et al.* [2008] also noted pronounced differences for different NAO phases, with less precipitation overall but an increased moisture contribution from the Norwegian Sea occurring for the positive NAO phase. In Norway, which is located on the eastern side of the average position of the Icelandic low, the effect of the NAO is just the opposite, namely to enhance precipitation and the importance of low-latitude moisture source regions during the positive NAO phase.

5. Conclusions

[33] We have studied an extreme precipitation event on the Norwegian southwest coast, which produced flooding and landslides and caused considerable infrastructure damage and loss of human life. We found that this event was triggered by the transport of (sub)tropical moisture associated with two former hurricanes, Maria [*Pasch and Blake*, 2006] and Nate [*Stewart*, 2005]. Both hurricanes underwent transition into extratropical cyclones and crossed the North Atlantic Ocean from west to east. The two hurricanes, which were traveling relatively close to each other, generated a large combined stream of (sub)tropical air toward the high latitudes. Most of the (sub)tropical moisture was originally associated with the hurricane Nate but it was incorporated into the circulation of former hurricane Maria located to the northeast of Nate, which transported the moist air even further north. This generated an atmospheric river [*Newell et al.*, 1992] rooted in the tropical western North Atlantic and ending at the Norwegian southwest coast. The steep topography of the Norwegian coast caused strong orographic enhancement of the precipitation associated with the river, a situation which is reminiscent of the atmospheric rivers impinging on the coast of California [*Ralph et al.*, 2004, 2005; *Bao et al.*, 2006]. The desiccation of the air by the strong precipitation terminated the river over Norway.

[34] To date, bands of large VIWV flux, called atmospheric rivers or moisture conveyor belts, have only been related to extratropical cyclones [*Ralph et al.*, 2004, 2005; *Bao et al.*, 2006] or cut-off lows in the subtropics [*Knippertz and Martin*, 2007]. In this paper, we have shown that such bands of large VIWV fluxes can also be produced by hurricanes undergoing extratropical transition.

[35] We employed a Lagrangian moisture tracking algorithm [*Stohl and James*, 2004, 2005] to show that the evaporative source of the precipitation falling over Norway during the event was mostly subtropical with contributions also from the tropics. Through convergence, water originating from relatively close-by midlatitude source regions was incorporated into the precipitating airstream, too. A tropical moisture source has also been reported for atmospheric rivers over California which, however, is located more than 20° further south. In our case, some of the moisture was transported across more than 40° of latitude.

[36] By applying the moisture tracking algorithm also over a 5-year period, we found that tropical and subtropical source regions can contribute moisture for precipitation over southwestern Norway throughout the year. Thus other mechanisms than hurricanes must also be responsible for transporting tropical moisture toward Norway, but these need to be studied further. Precipitation amounts in southwestern Norway were larger and the importance of low-latitude moisture source regions was enhanced for a winter with a positive NAO phase, as compared to a winter with a negative NAO phase. The relative moisture contribution of (sub)tropical source regions was also larger for stronger precipitation events than for weaker ones.

[37] Precipitation amounts in southwestern Norway have increased [*Hanssen-Bauer*, 2005] and heavy precipitation events have become more frequent [*Groisman et al.*, 1999] over the last century. Climate model predictions suggest that these trends will continue in the future and will be strongest in fall [*Benestad*, 2005; *Hanssen-Bauer et al.*, 2003]. Although this is still debated [*Pielke et al.*, 2005], some scholars [e.g., *Emanuel*, 2005] suggest a positive trend in various measures of hurricane frequency and intensity. Our study suggests that such a trend, if real and continuing into the future, would be of significance not only for those regions directly impacted by landfalling hurricanes but also for high-latitude regions. Although climate models do not resolve individual hurricanes, it is intriguing to think that the predicted strong precipitation increase in southwestern Norway in fall could be related to an enhanced transport of (sub)tropical moisture toward Norway.

[38] **Acknowledgments.** This study was supported by the Norwegian Research Council as part of the projects "Where Norway receives its water from" (project 172707/S30) and POCAHONTAS (project 178345/S30). We thank the Norwegian Meteorological Institute for the precipitation radar image (Figure 1) taken from their website as well as for the precipitation data measured at various stations. Meteosat satellite data were provided by EUMETSAT, and H. Mannstein and S. Rentsch (German Aerospace Center) provided guidance for plotting these data. We thank H. Huntrieser and two anonymour reviewers for comments on the paper, which helped improving its quality.

References

Alfnes, E., and E. J. Førland (2006), Trends in extreme precipitation and return values in Norway 1900–2004, Norwegian Meteorological Institute Report 2/2006, Oslo.

Bao, J.-W., S. A. Michelson, P. J. Neiman, F. M. Ralph, and J. M. Wilczak (2006), Interpretation of enhanced integrated water vapor bands associated with extratropical cyclones: Their formation and connection to tropical moisture, *Mon. Weather Rev.*, *134*, 1063–1080.

Benestad, R. E. (2005), Climate change scenarios for northern Europe from multi-model IPCC AR4 climate simulations, *Geophys. Res. Lett.*, *32*, L17704, doi:10.1029/2005GL023401.

Eckhardt, S., A. Stohl, H. Wernli, P. James, C. Forster, and N. Spichtinger (2004), A 15-year climatology of warm conveyor belts, *J. Clim.*, *17*, 218–237.

ECMWF (2002), IFS Documentation, edited by P. W. White, ECMWF, Reading, UK.

Eltahir, E. A. B., and R. L. Bras (1996), Precipitation recycling, *Rev. Geophys.*, *34*, 367–378.

Emanuel, K. (2005), Increasing destructiveness of tropical cyclones over the past 30 years, *Nature*, *436*, 686–688.

Groisman, P. Y. A., et al. (1999), Changes in the probability of heavy precipitation: Important indicators of climate change, *Clim. Change*, *42*, 243–283.

Hanssen-Bauer, I. (2005), Regional temperature and precipitation series for Norway: Analyses of time-series updated to 2004, Norwegian Meteorological Institute Report 15/2005, Oslo.

Hanssen-Bauer, I., E. J. Førland, J. E. Haugen, and O. E. Tveito (2003), Temperature and precipitation scenarios for Norway: Comparison of results from empirical and dynamical downscaling, Norwegian Meteorological Institute Report 06/2003, Oslo.

Hurrell, J. W. (1995), Decadal trends in the North Atlantic Oscillation: Regional temperatures and precipitation, *Science*, *269*, 676–679.

Knippertz, P., and J. E. Martin (2007), A Pacific moisture conveyor belt and its relationship to a significant precipitation event in the semiarid southwestern United States, *Weather Forecasting*, *22*, 125–144.

Meteorological Institute (2005), Weather in Norway - climatological monthly overview for September 2005 (in Norwegian), met.no info 09/2005, Oslo.

Newell, R. E., N. E. Newell, Y. Zhu, and C. Scott (1992), Tropospheric rivers?–A pilot study, *Geophys. Res. Lett.*, *19*, 2401–2404.

Nieto, R., L. Gimeno, and R. Trigo (2006), A Lagrangian identification of major sources of Sahel moisture, *Geophys. Res. Lett.*, *33*, L18707, doi:10.1029/2006GL027232.

Nieto, R., L. Gimeno, D. Gallego, and R. Trigo (2007), Contributions to the moisture budget of airmasses over Iceland, *Meteorol. Z.*, *16*, 37–44.

Pasch, R. J., and E. S. Blake (2006), Tropical cyclone report-hurricane Maria, National Hurricane Center, 9 p., February 2006.

Pielke, R. A., C. Landsea, M. Mayfield, J. Laver, and R. Pasch (2005), Hurricanes and global warming, *Bull. Am. Meteorol. Soc.*, *86*, 1571–1575.

Ralph, F. M., P. J. Neiman, and G. A. Wick (2004), Satellite and CALJET aircraft observations of atmospheric rivers over the eastern North Pacific Ocean during the winter of 1997/98, *Mon. Weather Rev.*, *132*, 1721–1745.

Ralph, F. M., P. J. Neiman, and R. Rotunno (2005), Dropsonde observations in low-level jets over the Northeastern Pacific Ocean from CALJET-1998 and PACJET-2001: Mean vertical-profile and atmospheric-river characteristics, *Mon. Weather Rev.*, *133*, 889–910.

Ralph, F. M., P. J. Neiman, G. A. Wick, S. I. Gutman, M. D. Dettinger, D. R. Cayan, and A. B. White (2006), Flooding on California's Russian River: Role of atmospheric rivers, *Geophys. Res. Lett.*, *33*, L13801, doi:10.1029/2006GL026689.

Sodemann, H., C. Schwierz, and H. Wernli (2008), Interannual variability of Greenland winter precipitation sources: Lagrangian moisture diagnostic and North Atlantic Oscillation influence, *J. Geophys. Res.*, *113*, D03107, doi:10.1029/2007JD008503.

Stewart, S. R. (2005), Tropical cyclone report - hurricane Nate, National Hurricane Center, 11 p., November 2005.

Stohl, A. (2006), Characteristics of atmospheric transport into the Arctic troposphere, *J. Geophys. Res.*, *111*, D11306, doi:10.1029/2005JD006888.

Stohl, A., and P. James (2004), A Lagrangian analysis of the atmospheric branch of the global water cycle: 1. Method description, validation, and demonstration for the August 2002 flooding in Central Europe, *J. Hydrometeorol.*, *5*, 656–678.

Stohl, A., and P. James (2005), A Lagrangian analysis of the atmospheric branch of the global water cycle: 2. Earth's river catchments, ocean basins, and moisture transports between them, *J. Hydrometeorol.*, *6*, 961–984.

Stohl, A., M. Hittenberger, and G. Wotawa (1998), Validation of the Lagrangian particle dispersion model FLEXPART against large scale tracer experiment data, *Atmos. Environ.*, *32*, 4245–4264.

Stohl, A., C. Forster, A. Frank, P. Seibert, and G. Wotawa (2005), Technical note: The Lagrangian particle dispersion model FLEXPART version 6.2., *Atmos. Chem. Phys.*, *5*, 2461–2474.

Trenberth, K. E., and C. J. Guillemot (1998), Evaluation of the atmospheric moisture and hydrological cycle in the NCEP/NCAR reanalyses, *Clim. Dyn.*, *14*, 213–231.

Uvo, C. B. (2003), Analysis and regionalization of Northern European winter precipitation based on its relationship with the North Atlantic Oscillation, *Int. J. Clim.*, *23*, 1185–1194.

Wentz, F. J., and R. W. Spencer (1998), SSM/I rain retrievals within a unified all-weather ocean algorithm, *J. Atmos. Sci.*, *55*, 1613–1627.

Wernli, H. (1997), A Lagrangian-based analysis of extratropical cyclones. II: A detailed case-study, *Q. J. R. Meteorol. Soc.*, *123*, 1677–1706.

Wernli, H., S. Dirren, M. A. Liniger, and M. Zillig (2002), Dynamical aspects of the life cycle of the winter storm 'Lothar' (24–26 December 1999), *Q. J. R. Meteorol. Soc.*, *128*, 405–429.

Zhu, Y., and R. E. Newell (1998), A proposed algorithm for moisture fluxes from atmospheric rivers, *Mon. Weather Rev.*, *126*, 725–735.

C. Forster, Institute for Atmospheric Physics, German Aerospace Center, Oberpfaffenhofen, Germany.

H. Sodemann and A. Stohl, Norwegian Institute for Air Research (NILU), Instituttveien 18, 2027 Kjeller, Norway. (ast@nilu.no)